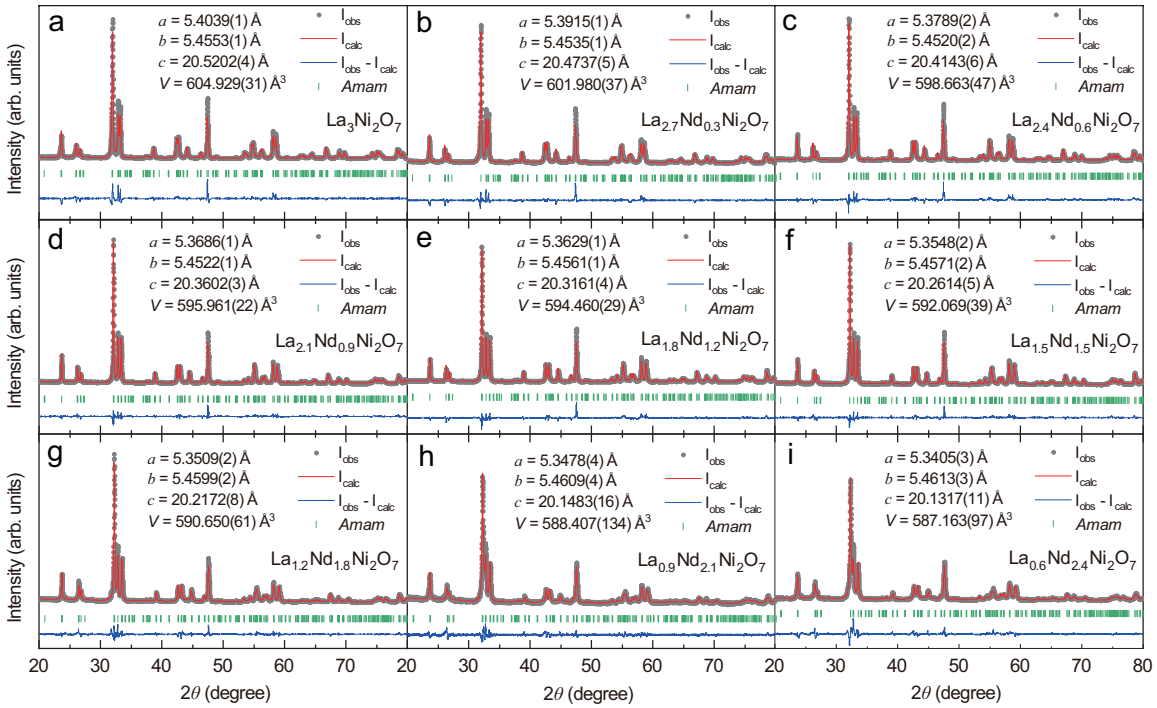
Supplymentary Information for

High-Temperature superconductivity at 100 K in $La_{3-x}Nd_xNi_2O_7$

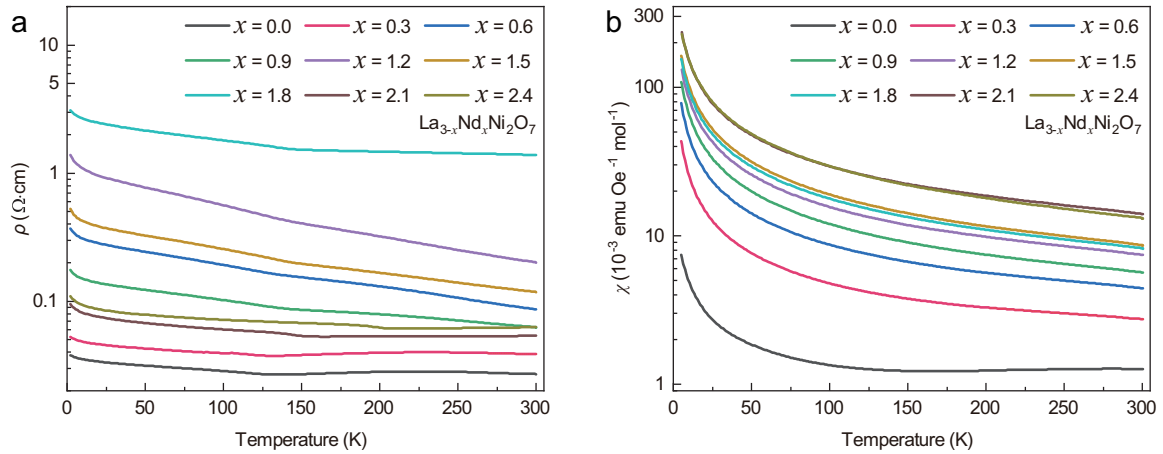
Zhengyang Qiu[1†], Junfeng Chen[1†], Dmitrii V. Semenok[2†], Qingyi Zhong[3], Di Zhou[2], Jingyuan Li[1], Peiyue Ma[1], Xing Huang[1], Mengwu Huo[1], Tao Xie[1], Xiang Chen[1], Ho-kwang Mao[4,5], Viktor V Struzhkin[4,5*], Hualei Sun[3,1*], Meng Wang[1*]

[1]Center for Neutron Science and Technology at School of Physics, Guangdong Provincial Key Laboratory of Magnetoelectric Physics and Devices, Sun Yat-Sen University, Guangzhou, 510275, Guangdong, China.
[2]Center for High Pressure Science and Technology Advanced Research (HPSTAR), Beijing, 100193, China.
[3]School of Science, Sun Yat-Sen University, Shenzhen, 518107, Guangdong, China.
[4]Center for High Pressure Science and Technology Advanced Research (HPSTAR), Shanghai, 201203, China.
[5]Shanghai Key Laboratory of Material Frontiers Research in Extreme Environments (MFree), Shanghai Advanced Research in Physical Sciences (SHARPS), Pudong, Shanghai, 201203, China.

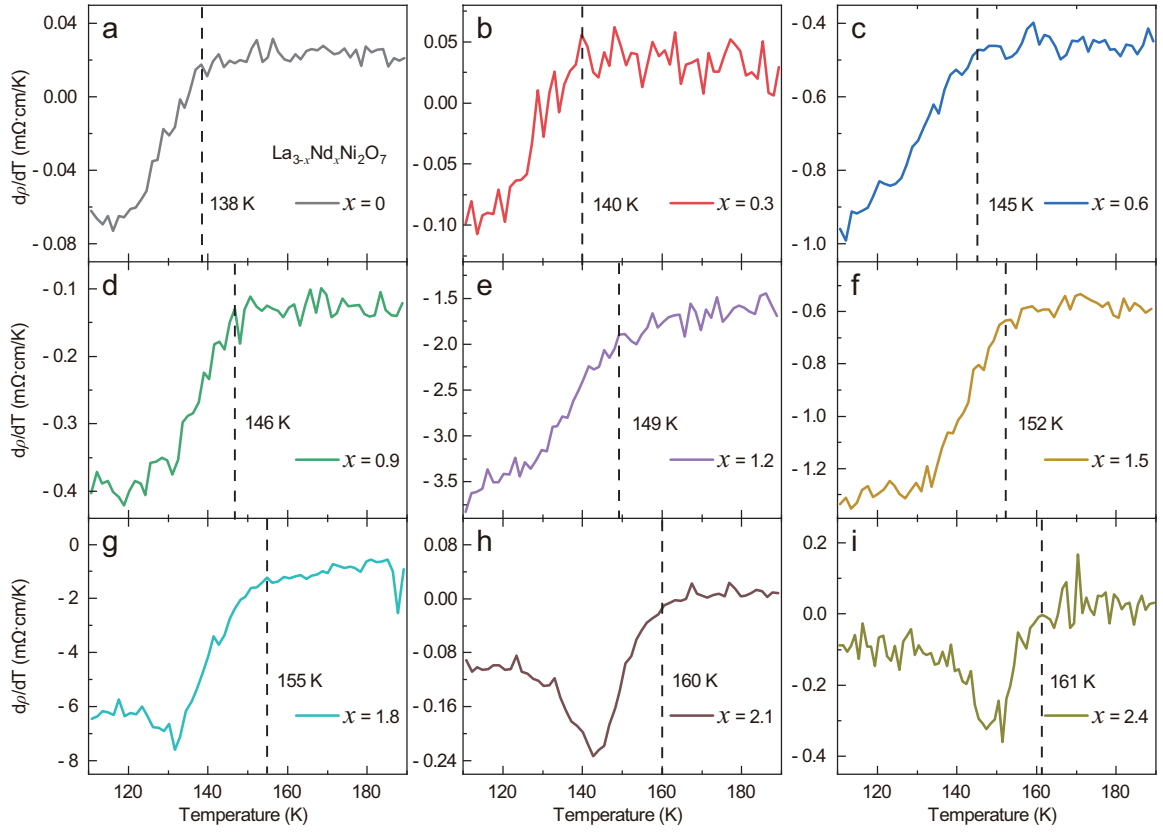
*Corresponding author(s). E-mail(s): viktor.struzhkin@hpstar.ac.cn; sunhlei@mail.sysu.edu.cn; wangmeng5@mail.sysu.edu.cn;
†These authors contributed equally to this work.



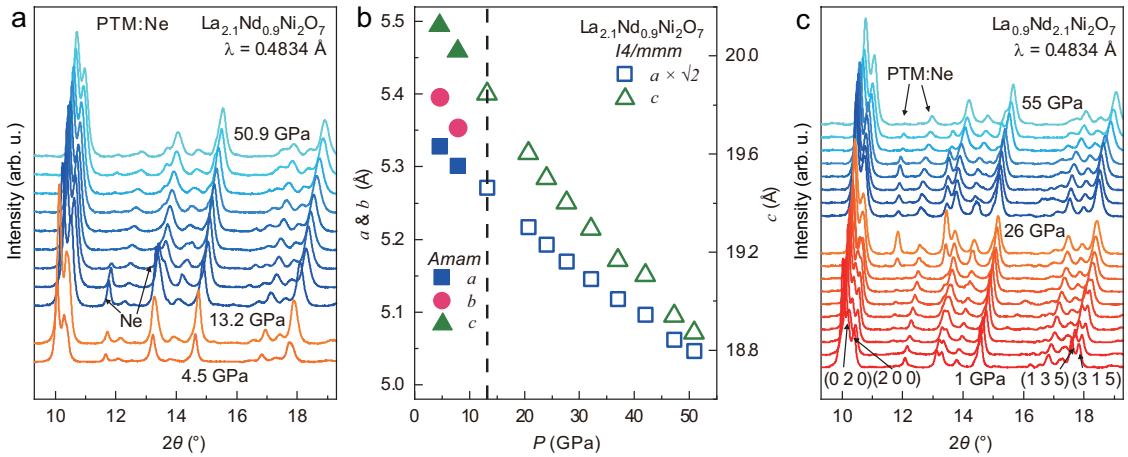
Supplementary Fig. 1 Rietveld refinements for the $La_{3-x}Nd_xNi_2O_7$ ($0 \leq x \leq 2.4$). The data were collected with an X-ray diffractometer at room temperature. The nominal compositions, refined parameters, and refined diffraction patterns have been presented in the figure.



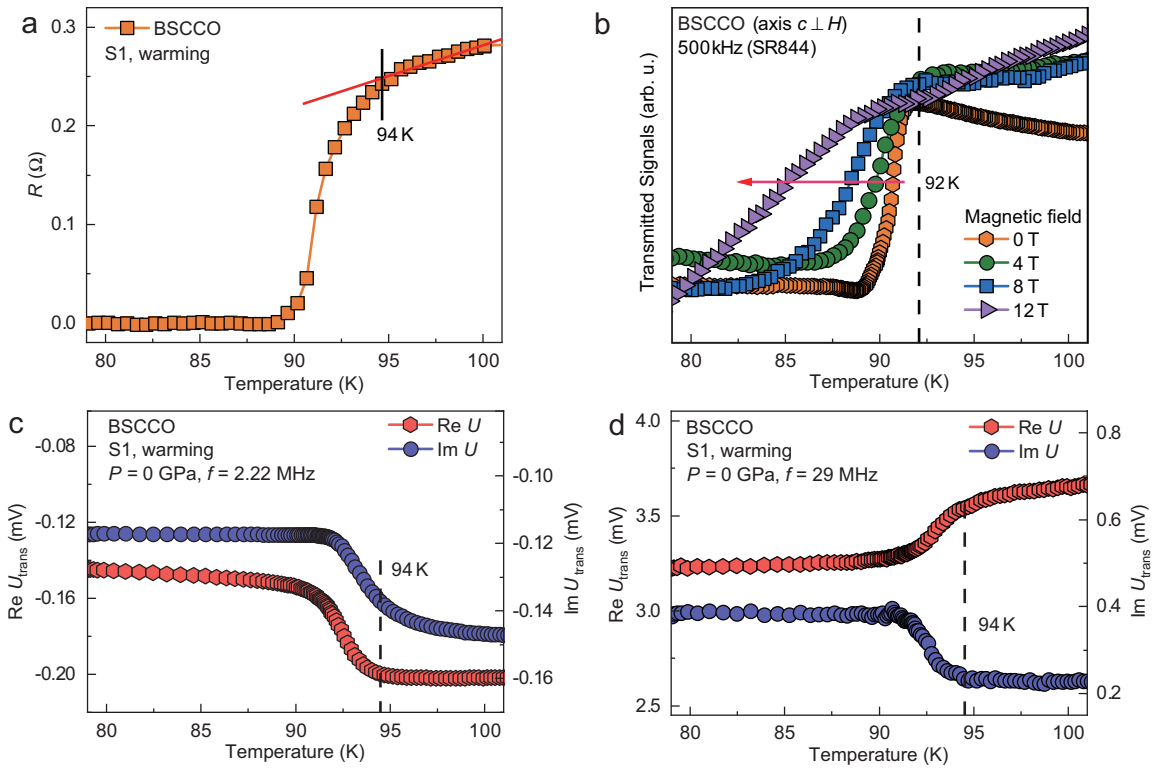
Supplementary Fig. 2. Resistivity and magnetic susceptibility of $La_{3-x}Nd_xNi_2O_7$ ($0 \leq x \leq 2.4$). a, $\rho(T)$ of $La_{3-x}Nd_xNi_2O_7$ ($0 \leq x \leq 2.4$). As Nd doping increases, the temperature dependence of $\rho(T)$ increases up to $x = 1.8$ then decreases. **b,** $\chi(T)$ of $La_{3-x}Nd_xNi_2O_7$ ($0 \leq x \leq 2.4$). The temperature dependence of $\chi(T)$ increases gradually with the Nd-doping content.



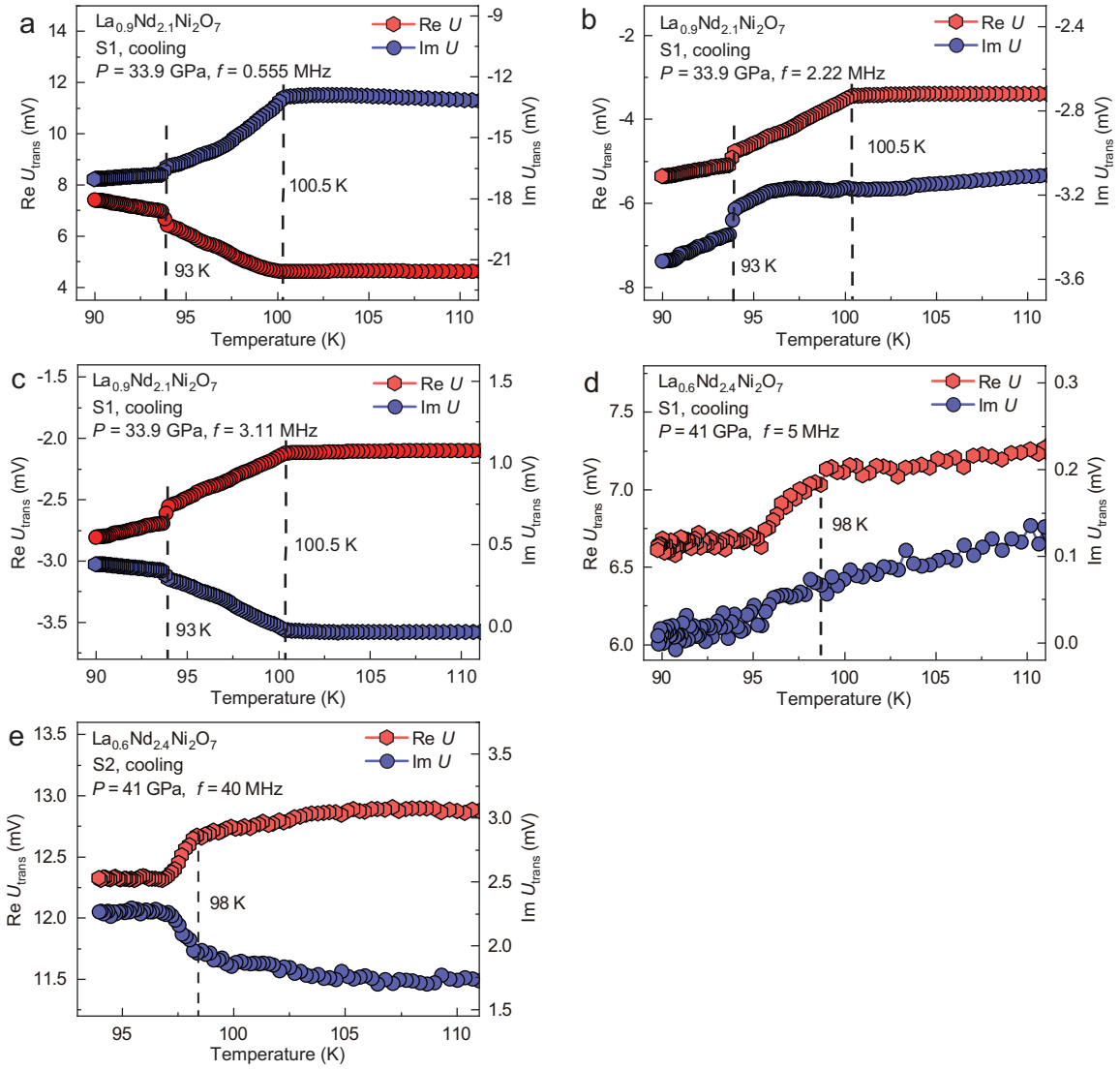
Supplementary Fig. 3. The derivative of $\rho(T)$ against temperature of $La_{3-x}Nd_xNi_2O_7$ ($0 \leq x \leq 2.4$). The dashed lines indicate the density wave transition temperature T_{SDW} for each composition. As Nd doping increases, the transition temperature T_{SDW} of $d\rho(T)/dT$ increases from 138 ± 5 K to 161 ± 6 K.



Supplementary Fig. 4. Synchrotron XRD measurements on $La_{2.1}Nd_{0.9}Ni_2O_7$ and $La_{0.9}Nd_{2.1}Ni_2O_7$. a, Room-temperature synchrotron XRD patterns on the $x = 0.9$ compound under different pressures. The structural transition from *Amam* to $I4/mmm$ occurs at 13.2 GPa. **b,** Lattice parameters of a, b, and c refined from synchrotron XRD patterns as a function of pressure. Solid symbols represent lattice parameters in the *Amam* space group while hollow symbols represent lattice parameters in the $I4/mmm$ space group. **c,** Identical XRD patterns on the $x = 2.1$ compound under various pressures. The structural transition from *Amam* to $I4/mmm$ occurs at 26 GPa.



Supplementary Fig. 5. Resistance transportation and Radio-frequency transmission measurements for a BSCCO reference film. a, The $R(T)$ curve of the BSCCO reference sample. RF measurements for the BSCCO; **b,** in magnetic fields in Oxford magnet system; Real (Re U) and imaginary (Im U) components of the transmitted RF signal as a function of temperature for **c–d,** in zero magnetic field in a high-pressure diamond cell (microsample).



Supplementary Fig. 6. Radio-frequency transmission measurements for sample characterization. Real (Re U) and imaginary (Im U) components of the transmitted RF signal as a function of temperature for: **a–c,** the $La_{0.9}Nd_{2.1}Ni_2O_7$ sample under various conditions; **d–e,** $La_{0.6}Nd_{2.4}Ni_2O_7$ samples under different measurement protocols.